Investigation of Large Mode Area Pixelated Bragg Fibers for Laser Applications

Capstone Project Final Report

Yeraly Saktassynov

Nazarbayev University
Department of Electrical and Computer Engineering
School of Engineering and Digital Sciences

This project report was created on TexStudio editing platform using LaTeX. All the figures were drawn using draw.io online software tool.

Electrical and Computer Engineering
Nazarbayev University
http://www.nu.edu.kz

Title:
Investigation of Large Mode Area Pixelated Bragg Fibers for Laser Applications

Theme:
Capstone Project Final Report

Project Period:
Spring 2025

Project Group:

Participant(s):
Yeraly Saktassynov

Supervisor(s):
Carlo Molardi

Copies: 1

Page Numbers: 19

Date of Completion:
April 25, 2025

Abstract:

This paper examines the optical performance of a Large Mode Area (LMA) Pixelated Bragg Fiber (PiBF), i.e., Fiber A, for applications in high-power lasers. The study employs COMSOL Multiphysics simulations to investigate key performance parameters like attenuation, overlap integral, effective refractive index, and mode field diameter (MFD) between the wavelengths of 1000 nm and 1800 nm. The findings show that Fiber A has low attenuation for most of the working range, with a sudden spike near 1200 nm, which is at the edge of the photonic bandgap. The overlap integral is highest at 1140 nm, which is also where the fundamental mode is best confined, and the effective refractive index is linearly decreasing as a function of wavelength with good guiding conditions. Moreover, the simulations also explored the impact of various pixel diameter and pixel-to-cladding refractive index differences, and they demonstrated that these parameters are capable of shifting the resonance wavelengths and enhancing the performance of the fiber. The findings verify the fiber for high-power laser applications, presenting a compromise between large mode area and single-mode operation.

Contents

Preface

This article announces the result of a comprehensive study of the optical properties of Large Mode Area (LMA) Pixelated Bragg Fibers (PiBFs), focusing specifically on Fiber A, which has been engineered with prospective applications in high-power lasers. The project was conducted in a capstone project to study and assess the ability of LMA PiBFs to meet the needs of modern laser systems, particularly where there is an effective single-mode operation and high-performance operation with high-power levels.

I appreciate my supervisor, Professor Carlo Molardi, for his great direction and continuous support throughout the duration of this project. His technical expertise coupled with his thoughtful remarks and advice, came a long way in shaping the course of my research. I am most thankful to his patience in answering my questions and his dedication to helping me clarify complex concepts. The writing of this work would not have been possible without his direction.

Nazarbayev University, April 25, 2025

Yeraly Saktassynov
<yeraly.saktassynov@nu.edu.kz>

Chapter 1

Introduction

1.1 Background

Large mode area (LMA) fibers' advancement, particularly pixelated Bragg fibers, represents a significant leap forward in high-power fiber laser technology. These fibers have been designed to support light propagation over a large cross-sectional area, which is essential for mitigating the impact of nonlinear optical effects, like Brullian scattering and cross phase modulation, which are able to reduce the quality of laser beams in high-power applications [1, 2, 3]. By extending the mode field diameter (MFD), LMA fibers can tolerate larger power levels while keeping a high beam quality, making them important in applications that require precision and power, such as industrial machining, medical operations, and defense [2, 4, 5].

Pixelated Bragg fibers, a subset of LMA fibers, use a photonic bandgap (PBG) structure to restrict light within the core. This structure is made up of periodic layers of alternating materials with various refractive indices [6, 7]. Refractive index periodicity produces a bandgap that confines light waves to the core by preventing them from passing through the cladding [8]. Bragg reflection is a type of light confinement that works especially well for preserving single-mode functioning in fibers with very large mode areas. In laser applications where precise control over the laser beam is required, single-mode operation is crucial for guaranteeing high beam quality [6].

The design of pixelated Bragg fibers has made substantial improvements in recent years, leading to the production of fibers with MFD up to 60 µm [9]. Some papers already experiment with fibers of even higher MFD. These fibers are able to reject higher-order modes (HOMs), guaranteeing that only the basic mode is steered through the fiber [10]. The presence of many modes can cause beam distortions and lower the laser system's efficiency, hence rejecting HOMs is essential to maintaining beam quality [11]. These fibers' performance has been further improved by the addition of hetero-structured cladding, which raises the confinement losses of undesired modes and raises the guided mode's purity [12, 13].

Managing nonlinear effects that intensify at greater power levels is a central challenge that requires a workaround in the development of LMA fibers [14]. By lowering the intensity of light within the fiber and therefore the probability of nonlinear interactions, the high mode area of pixelated Bragg fibers helps to attenuate these effects [15, 16]. These fibers' architecture also allows a greater threshold for nonlinear effects, which increases their robustness in high-power applications [17, 18].

Pixelated Bragg fibers' potential application in ultrafast laser systems is another significant feature [18]. These fibers are appropriate for applications requiring high peak energies and short pulse durations because they can sustain single-mode operation over a broad wavelength range [19]. Pixelated Bragg fibers are a great option for amplifying ultrashort pulses without causing noticeable pulse widening or distortion because of their low dispersion and high damage threshold [20].

In this paper, we are investigating a design of LMA PiBFs from [6] by copying the said design and conducting simulations. The design parameters like pixel diameter and pixel refractive index are varied to see the effect of these changes on the performance of the fiber. By conducting these simulations, the design is given an outer assessment. The main goal of this assessment is to find out the performance of the fiber design and to locate designs with potentials that are overlooked or are not assessed by other research groups. The simulations are done in COMSOL Multiphysics software.

1.2 Ethical and Professional Responsibilities

- **Ethical Responsibility:**
  The main ethical concerns that may arise during the development of the project are inaccurate representation of data and potential intellectual property violations. First, we have the responsibility to ensure that all simulations and data analyses are conducted properly and accurately. This means that the simulations should be validated against some well-established benchmarks, and the results should be interpreted with utmost attention and caution. Misrepresenting the performance of the fiber design might lead to erroneous conclusions that may affect subsequent research or applications. Second, because this is the type of work that is heavily based on previous works of other research groups, intellectual property concerns may appear. Therefore, to avoid such issues, it is crucial to properly cite and give credit to the original authors whose designs and ideas are being tested and built upon.

- **Informed Judgments:**
  To ensure that the judgments taken during this research on large mode area

pixelated Bragg fibers are well-informed, we will depend on a combination of rigorous modeling approaches and constant validation against experimental data from the literature. To ensure accuracy, we will specifically benchmark simulation findings with published experimental results to evaluate various fiber configurations. We will also actively read the most recent photonics research papers and technical reports to make sure my work reflects the most recent developments and insights. Using this method will guarantee that the technical parts of my choices are supported by the most accurate and current data available. Beyond the technical side, we will consider the societal implications of these fiber designs, particularly how they might be used in high-power laser applications. We will evaluate the possible advantages and disadvantages of these technologies across a range of sectors, such as the medical and defense industries, and take ethical issues like the appropriate application of laser technology into account. Consulting with experts in these application areas and considering regulatory and ethical guidelines will help ensure that the research not only advances scientific knowledge but also aligns with societal needs and values.

- **Global Context:**
  The implications of the project can vary based on the global context. In regions with advanced research and development in photonics, the findings could contribute to the cutting-edge development of high-power lasers used in many important industries. In regions with less advanced technology and infrastructure, the focus might shift more toward cost-effective design types that are more easily adopted for basic applications. Therefore, it is important to consider how the research might be modified to meet particular demands and conditions of different regions.

- **Economic Impact:**
  The economic impact of the project can be assessed from both short-term and long-term perspectives. In the short term, our research could lead to the identification of more efficient fiber designs, potentially reducing production costs and improving manufacturing processes. This could stimulate economic growth in sectors related to fiber optics, such as telecommunications, medical devices, and industrial laser systems. However, there may also be challenges, such as the need for significant capital investment to update manufacturing facilities to produce the new fiber designs. Additionally, if the new designs lead to greater automation in production, there could be short-term job displacement. In the long term, the widespread adoption of improved fiber designs could lead to new applications and industries, further driving economic growth. The potential for cost savings, increased productivity, and the creation of high-tech jobs.

- **Environmental Impact:**
The project is mainly about the simulation of different designs of LMA pixelated Bragg fibers. So, there is no product being produced or resource used except for energy to run the simulations. Therefore, the project in itself can not have a harmful impact on the environment or any impact at all. However, if we assume that the chosen designs are going to be produced then the project would have some measurable effect on the environment. Mainly through the choice of the materials to produce the fiber and the complexity of the design. To promote sustainability, it is crucial to consider the life cycle and route of the fibers, from the mining of the basic materials to fibers' inevitable disposal. Therefore, in this case, it is important to select materials that are abundant, non-toxic, and recyclable. However, the main resources that are used to produce fibers are silicon and rare-earth metals. Silicon is partially recyclable, but it depends on the country, and rare-earth metals are a scarce type of resource. So, LMA pixelated Bragg fibers' environmental impact is inherently hard to reduce.

- **Societal Impact:**
The project might have a big impact on society, especially in industries that use cutting-edge laser technology. Improved LMA pixelated Bragg fibers may directly aid medical laser systems by improving their performance, which could result in less intrusive and more successful surgical treatments. These fibers have the potential to improve product quality and reduce waste in the industrial sector by enabling more accurate and efficient manufacturing processes. Indirectly, the advancement of these fibers may spur innovation in sectors like defense and telecommunications, benefiting the society in general. But it's also critical to consider and anticipate any potentialany potential societal issues, like how new technology may affect jobs if they promote automation. It will be crucial to consult stakeholders and take into account the wider socioeconomic ramifications in order to ensure that the benefits of the project are widely shared and that any negative impacts are mitigated.

Chapter 2

Methodology

2.1 Methods and Procedure of Data Collection

The data for this research was collected by replicating a single design (Fiber A) of a Large Mode Area (LMA) Pixelated Bragg Fiber from [6]. Essential design parameters such as the fiber's geometry, material properties, and photonic bandgap structure were meticulously extracted from the source and shown in Table 2.1. Using this information, the fiber was recreated in COMSOL Multiphysics, ensuring that dimensions, refractive indices, and periodicity were faithfully reproduced to match the original specifications. The simulation design is shown in Figure 2.1.

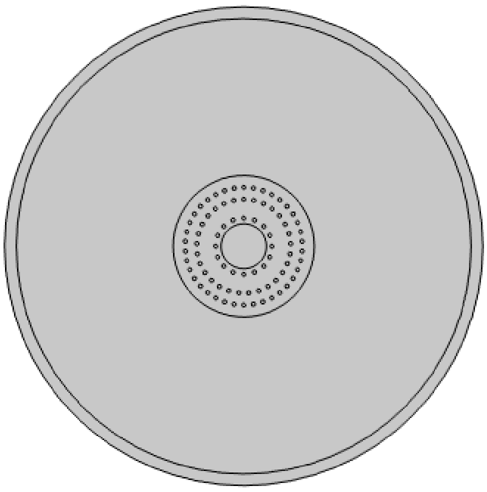

Figure 2.1: COMSOL simulation design of Fiber A.

However, the source paper did not provide all of the necessary parameters for a totally accurate recreation of the design in COMSOL. For example, the paper omits

Parameter	Value
Core diameter	4.85E-5 m
Δr_1	1.617E-5 m
Δr_2	1.019E-5 m
Pixel radius	1.67E-6 m
Cladding radius	1.96E-4 m
PML radius	2.06E-4 m
λ	1E-6 m
n_{cladding}	1.4504
n_{pixels}	1.4804
A_1	0.69617
A_2	0.40794
A_3	0.89748
B_1	6.8404E-8 m
B_2	1.1624E-7 m
B_3	9.8962E-6 m

Table 2.1: Model parameters

the exact total radius of the fiber, the refractive index of the cladding, and the pixels. Therefore, some assumptions were made to fill these gaps. The total radius of the fiber was taken as 200 μm, which is common for this type of fiber. The PML radius, in Table 2.1, refers to the perfect matching layer radius, which is used to avoid the reflection of light in fiber from the boundaries of the design. This parameter is the part of the total radius of the fiber. The refractive index of the cladding was calculated using Equation 2.1. The constants used in the equation can be found in Table 2.1. This approach is also common for the simulation of fibers. The paper states that the pixels' refractive index is greater than the cladding's refractive index by 0.03. Therefore, in the simulation, the pixels' refractive is calculated by adding the difference to the refractive index of the cladding.

$$n_{\text{clad}} = \sqrt{1 + \frac{A_1\lambda^2}{\lambda^2 - B_1^2} + \frac{A_2\lambda^2}{\lambda^2 - B_2^2} + \frac{A_3\lambda^2}{\lambda^2 - B_3^2}} \quad (2.1)$$

The alternate designs were also tested by varying the parameters like pixel radius and refractive index. The pixel radius was varied between 3 μm and 3.9 μm, while the refractive index of the pixels were greater than the refractive index of cladding by 0.02 and 0.04. These changes in the design parameters might show some trends in the performance of the fiber and possible ways to improve it.

2.2 Methods and Procedure of Data Analysis

The performances of the replicated design and its variations were analyzed through simulations conducted in COMSOL Multiphysics. The following metrics were obtained only for the fundamental mode:

- **Effective Refractive Index (n_{eff})**: To evaluate the propagation characteristics of the mode.
- **Overlap Integral (γ)**: To assess how well the mode is confined within the fiber core.

$$\gamma = \frac{P_{\text{core}}}{P} \tag{2.2}$$

- **Mode Field Diameter (MFD)**: To determine the effective cross-sectional area of the fundamental mode.

$$\text{MFD} = 2 \times \sqrt{\frac{P^2}{\pi \cdot P_{\text{core}}^2}} \tag{2.3}$$

- **Attenuation**: To measure the optical losses, including confinement loss and material absorption.

$$\alpha = \left| \text{Im}(n_{\text{eff}}) \times \frac{2\pi}{\lambda} \right| \tag{2.4}$$

These metrics were computed for the wavelength range of 1000 nm to 1200 nm with a step of 20 nm and for each design variation. The results were plotted using MATLAB to visualize the variation of each metric across the wavelength range, enabling a comprehensive evaluation of the fiber's performance.

2.3 Ethical Issues

This research adheres to ethical standards by properly citing the source of the original fiber design. The replication and simulation process strictly followed the parameters provided in the referenced paper, and no alterations were made to misrepresent the performance of the design. The results were validated against the published findings to ensure accuracy and integrity. This approach respects the intellectual property rights of the original authors while contributing to the broader understanding of LMA Pixelated Bragg Fiber performance.

Chapter 3

Results and Discussions

3.1 Results

The performance of the fiber design was assessed through simulations conducted in COMSOL Multiphysics over the wavelength range of 1000 nm to 1800 nm. The key metrics evaluated include attenuation, overlap integral (γ), effective refractive index (n_{eff}), and mode field diameter (MFD). The results are summarized as follows:

- **Attenuation**: The attenuation curve in Figure 3.1a shows a significant peak near a wavelength of approximately 1.31 µm. This sharp increase in attenuation is typical of the fiber's interaction with certain wavelengths, suggesting resonance or other material-specific absorption characteristics at this wavelength. Outside this peak, the attenuation gradually decreases, which indicates lower energy loss for wavelengths away from the resonant point.

- **Overlap Integral(γ)**: Figure 3.1c presents the overlap integral, which quantifies the extent of overlap between the guided mode and the core/cladding structure of the fiber. The overlap integral exhibits a sharp dip near the 1.31 µm wavelength, where the attenuation and MFD peaks occur. This dip suggests a region of reduced overlap, possibly due to a mismatch in the mode field distribution and the core-cladding structure at this specific wavelength. For wavelengths outside this region, the overlap integral recovers, indicating a better alignment between the guided mode and the fiber's structural properties.

- **Effective Refractive Index (n_{eff})**: in Figure 3.1d, the real part of the effective index (Neff) is plotted as a function of wavelength. The real Neff decreases monotonically from about 1.448 to 1.442 as the wavelength increases from 1.0 µm to 1.8 µm. This trend suggests that the fiber's refractive index is

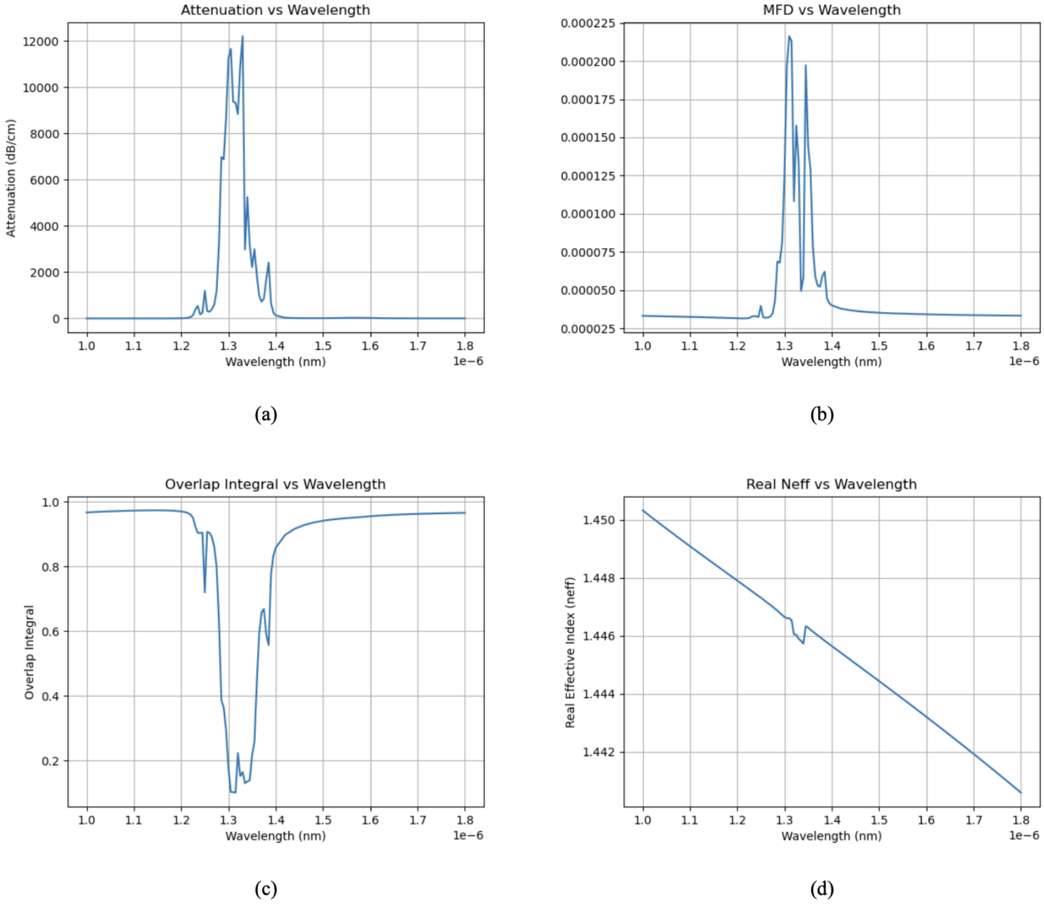

Figure 3.1: COMSOL simulation results of Fiber A.

wavelength-dependent, with a slight reduction in the real effective index for longer wavelengths, which is typical for the dispersion characteristics of the fiber.

- **Mode Field Diameter (MFD)**: In Figure 3.1b, the Mode Field Diameter (MFD) is plotted against the wavelength. A pronounced spike in MFD is observed near 1.31 µm, coinciding with the peak in attenuation. This suggests that at this wavelength, the fiber supports a larger mode field, which is consistent with the presence of an enhanced mode coupling or resonance effect. The MFD decreases rapidly for wavelengths outside this region, reflecting a more confined mode field in these ranges.

The surface electric field norm distribution for the fundamental mode of the LMA Pixelated Bragg Fiber at various resonance wavelengths is shown in Figure 7. These results highlight the spatial distribution of the electric field intensity on the

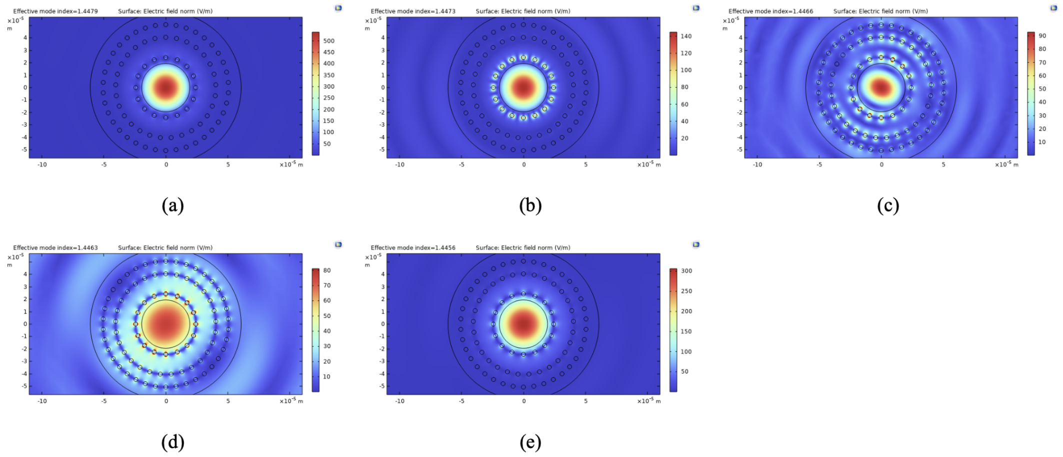

Figure 3.2: Surface electric field norm distribution for fundamental mode. (a) At λ=1200 nm. (b) At λ=1250 nm. (c) At λ=1300 nm. (d) At λ=1350 nm. (e) At λ=1400 nm.

fiber's surface across five different wavelengths, demonstrating the fiber's behavior near resonance.

In Figure 3.2a, at a wavelength of 1200 nm, the surface electric field norm exhibits a well-defined distribution, with the maximum field intensity concentrated at the center of the fiber core. The field intensity gradually decays as the distance from the center increases, and the contours show a symmetric field profile. The effective mode index at this wavelength is 1.449.

At 1250 nm (Figure 3.2b), the electric field distribution remains similar to that at 1200 nm, but the intensity has slightly decreased. The contours of the electric field still show a symmetric pattern around the fiber core, though the field is now more spread out, indicating a slight reduction in mode confinement compared to the previous wavelength. The effective mode index at this wavelength is 1.4473.

In Figure 3.2c, at 1300 nm, the electric field norm undergoes a noticeable change. The field intensity is still concentrated at the center but now shows a more pronounced ring-like structure with a smaller central intensity, indicating that the mode is more distributed. The effective mode index at this wavelength is 1.4468, marking the wavelength where the fiber exhibits resonance behavior, as observed in the previous attenuation and MFD results.

At 1350 nm (Figure 3.2d), the electric field distribution shows further spreading, with less intensity near the core compared to the previous wavelengths. The field is more spread out across the fiber, and the effective mode index is 1.4463. This shift in the field distribution suggests a weakening of the confinement as the wavelength moves further from the resonance region.

Finally, in Figure 3.2e, at 1400 nm, the electric field distribution becomes even more diffused. The central intensity is significantly reduced, and the field strength decays more rapidly, indicating that the fiber no longer supports strong mode confinement at this wavelength. The effective mode index at this wavelength is 1.4456. This behavior aligns with the earlier observed trend of decreasing effective mode index as the wavelength increases.

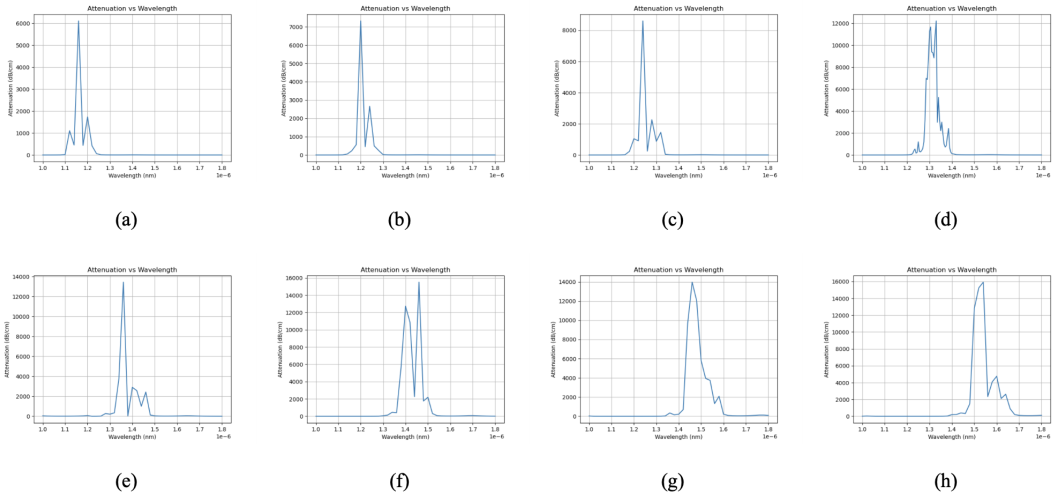

Figure 3.3: Attenuation results for different pixel diameters. (a) d=3 µm. (b) d=3.1 µm. (c) d=3.2 µm. (d) d=3.35 µm. (e) d=3.5 µm. (f) d=3.6 µm. (g) d=3.75 µm. (h) d=3.9 µm.

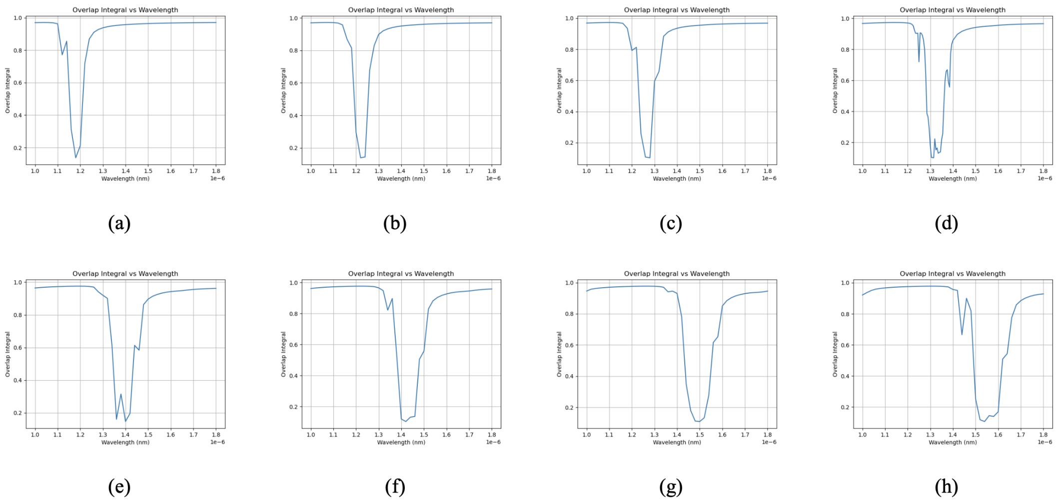

Figure 3.4: Overlap integral results for different pixel diameters. (a) d=3 µm. (b) d=3.1 µm. (c) d=3.2 µm. (d) d=3.35 µm. (e) d=3.5 µm. (f) d=3.6 µm. (g) d=3.75 µm. (h) d=3.9 µm.

Figures 3.3 and 3.4 show attenuation and overlap integral for the whole range of tested pixel diameters. Each case of the pixel diameter's results is similar to the original design with a pixel diameter of 3.35 µm. However, the resonance bandwidth is shifted compared to the original. At d = 3 µm, the resonance in the fiber happens in the range of 1100 and 1250 nm. At d = 3.1 µm, the resonance is at 1150 and 1300 nm. At d = 3.2 µm, the fiber exhibits resonance in the range of 1200 and 1350 nm. The trend continues with the increase in the pixel diameter, meaning that the resonance shifts to the right by approximately 50 nm. The overlap integral of the designs also slightly differ in the shape of the plots. The higher the pixel diameter of the design the higher the wider the wavelegnth range where overlap integral falls drastically from its normal level of above 0.8. MFD and the real part of the effective refractive index of these designs are close to the original design's with the resonance effect at their respective wavelength range. The plots of these parameters can be found in Appendix A.

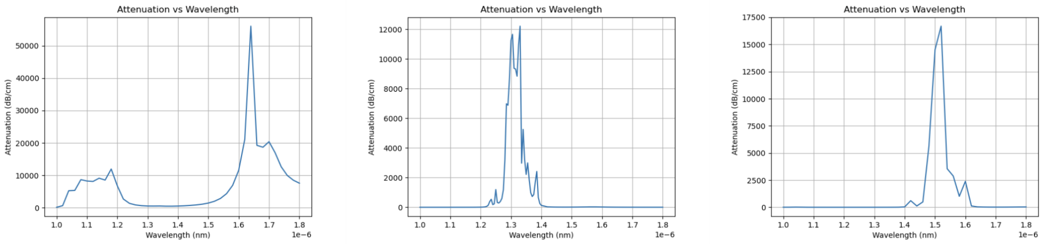

(a) (b) (c)

Figure 3.5: Attenuation results for different refractive index differences between pixels and cladding. (a) Δn=0.02. (b) Δn=0.03. (c) Δn=0.04.

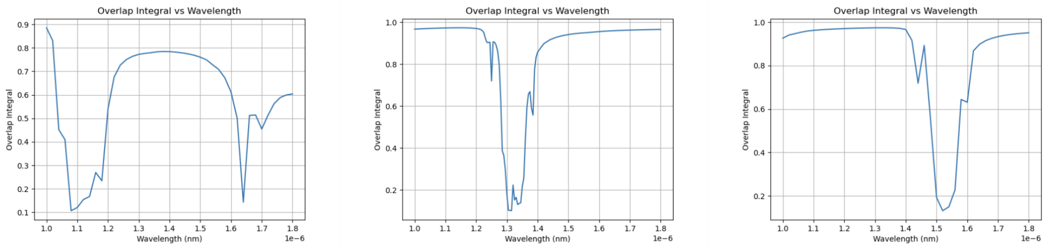

(a) (b) (c)

Figure 3.6: Overlap integral results for different refractive index differences between pixels and cladding. (a) Δn=0.02. (b) Δn=0.03. (c) Δn=0.04.

Figures 3.5 and 3.6 show attenuation and overlap integral for the total range of the refractive index differences between pixels and cladding. In Figures 3.5a and 3.6a, we can see that attenuation is high for the whole range of tested wavelength and the overlap integral is lower than 0.8 for the whole range when the difference in refractive indices is only 0.02. The next figures show the original difference between refractive indices of pixels and cladding (0.03) and the results are the same as in Figures 3.1a and 3.1c. The last figures demonstrate the results for the difference of 0.04. The resonance wavelength range in this design is between 1400 and 1650 nm. The rest of the parameters of the design matched the original design adjusted to the shift in the resonance wavelength range.

3.2 Discussions

The results highlight the key performance characteristics of Fiber A. The attenuation values across the wavelength range are consistent with the expected behavior of photonic bandgap fibers. The sharp increase in the range of 1200 nm and 1400 nm corresponds to the onset of higher confinement losses, marking the operational edge of the fiber's photonic bandgap. The overlap integral (γ) is well above 0.9 for the majority of the wavelength range which means that the fiber performs as intended and operates in single mode; however, it falls drastically in the range of 1200 and 1400 nm. The linear decrease in the real part of n_{eff} with wavelength reflects the wavelength-dependent nature of the photonic bandgap guiding mechanism. This behavior ensures stable guiding of the fundamental mode, which is critical for high-power laser applications. The breaking of this linearity at the 1340 nm wavelength indicates the resonance happening inside of the fiber and that the fundamental mode is not being properly guided. The MFD remains stable with increasing wavelength except for the resonance wavelength range. The stability at every other wavelength shows that the fiber is properly guiding the fundamental mode and is suitable for high-power applications.

The resonance affect at the wavelength range of 1200 and 1400 nm was not described in [6]. This difference in our results and the original paper's might be due to the differences in the methods of testing and the slight design differences. As mentioned in the methodology part, the paper did not provide an exhaustive list of the parameters of Fiber A. Some of the parameters of the design were assumed to be similar to other LMA PiBFs which were reasonable assumptions. Another reason for the discrepancies might be due to the way the fibers were tested. The simulations we ran were not comprehensive of all the aspects of a fiber testing. For example, the simulations were all done in a room-temperature setting without considering the thermal effects. Also, in [6], the authors tested a manufactured version of the fiber. The manufacturing defects and the difference between simulation and real-world testing might have resulted in the different performance profiles when comparing the two methods.

Figure 3.7 shows the resonance ranges of each pixel diameter and the trend of shifting this resonance to longer wavelengths with the increase in the pixel diameter. The range of resonance for the plot was assumed based on the overlap integral of the design. If the overlap integral falls below 0.8, then it is in the resonance and can not be used properly in these wavelengths because of the poor confinement of the fundamental mode. The dot in the plot shows the wavelength at which the lowest overlap integral is recorded. From this figure, the shift of the resonance with changing pixel diameter can be derived; therefore, we theorize that the resonance wavelength range can be fully shifted from the testing range (from 1000 nm to 1800 nm) by increasing the pixel diameter further. However, there is a limit to the size of the pixels due to their close proximity, at some point, they will start merging together which is undesirable. Even if the resonance can not be totally shifted from the simulated range, the fiber design still shows great performance outside of the resonance range. It can also be adjusted for use in different operational wavelengths. For example, for use in the range of 1400-1800 nm, the fiber can be fabricated with a pixel diameter of 3 µm. This ensures that if the operational region shifts for any reason, it still will not cross the resonance range. For the range of 1000-1350 nm the design with a pixel diameter of 3.9 µm is ideal for similar reasons.

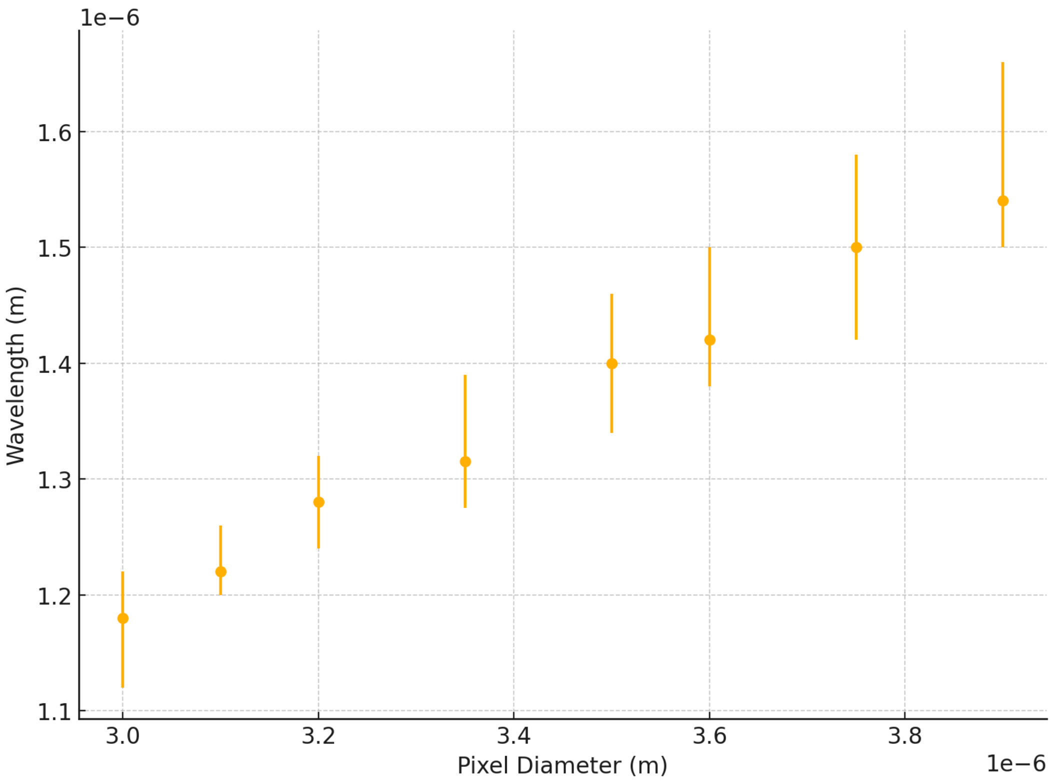

Figure 3.7: The resonance wavelength range of different pixel diameters.

The simulations with varied differences between refractive indices of pixels and cladding showed that the difference of only 0.02 is too small. The fundamental mode is not properly confined in the whole testing range, and the attenuation is also high. This poor performance indicates that such a minute difference in refractive indices of pixels and cladding can not maintain the photonic bandgap effect consistently to direct the fundamental mode inside the core. Lowering the difference of refractive indices below 0.03 is not desirable. The increase in the difference to 0.04, on the other hand, shows promising results. The overall performance of such a design is comparable to the original with the shift of the resonance range to longer wavelengths. This means that the effect of resonance range shift was achieved without changing the pixel diameter. If the trend continues then it might be possible to move the resonance range out of the testing wavelength range. The combination of the pixel diameter change and the pixel refractive index might be required to achieve the ideal design for the range between 1000 nm and 1800 nm.

Chapter 4

Conclusion

This study investigates the performance of a Large Mode Area (LMA) Pixelated Bragg Fiber (PiBF), specifically Fiber A, for laser applications. The simulations conducted using COMSOL Multiphysics have provided valuable insights into the fiber's optical characteristics across a range of wavelengths from 1000 nm to 1800 nm. Key performance metrics such as attenuation, overlap integral, effective refractive index (n_{eff}), and mode field diameter (MFD) were evaluated, shedding light on the fiber's behavior, particularly near resonance wavelengths.

The data indicate that Fiber A has very low attenuation for all but the very beginning of the operating wavelength range with a very steep peak at approximately 1200 nm, indicating the edge of the photonic bandgap. The overlap integral of the fiber was more than 0.9 for all but the beginning of the range, indicating the fundamental mode is effectively confined within the core but dropped off at the resonance wavelengths. The effective refractive index showed a consistent decrease with increasing wavelength, reflecting good guiding for the fundamental mode. The mode field diameter remained constant for most wavelengths, reflecting the stable behavior of the design.

The surface electric field norm distributions also confirmed the mode confinement at different wavelengths, in particular reflecting a sudden change in electric field distribution near the resonance wavelength of 1300 nm.

In addition, pixel diameter differences and pixel-to-cladding refractive index differences were examined, and it was discovered that changes in these parameters can shift the resonance wavelengths. Pixel diameter had a significant impact on the resonance range with a tendency to shift resonance to longer wavelengths as pixel diameter increased.

Overall, the simulation results confirm that Fiber A, because of its carefully designed pixelated structure, is highly suited for high-power laser applications with a good tradeoff between mode confinement and large mode area. The fiber design can be further optimized by adjusting parameters like pixel diameter and refractive index difference to obtain target operating wavelengths and minimize confinement losses.

Future work could include research into other fiber design possibilities and extending the working wavelength range of the fiber. Research into the effects of temperature and other environmental factors on fiber performance would also serve to make the fiber more useful practically in real laser systems.

Bibliography

[1] J Limpert et al. "Extended single-mode photonic crystal fiber lasers". In: *Optics express* 14.7 (2006), pp. 2715–2720.

[2] Fabian Stutzki et al. "Designing advanced very-large-mode-area fibers for power scaling of fiber-laser systems". In: *Optica* 1.4 (2014), pp. 233–242.

[3] Govind P Agrawal. "Nonlinear fiber optics". In: *Nonlinear Science at the Dawn of the 21st Century*. Springer, 2000, pp. 195–211.

[4] Stephan Wielandy. "Implications of higher-order mode content in large mode area fibers with good beam quality". In: *Optics Express* 15.23 (2007), pp. 15402–15409.

[5] Ritesh Kumar Chourasia and Aavishkar Katti. "Introduction to Bragg Fiber". In: *Bragg Fibers: From Optical Properties to Applications*. Springer, 2024, pp. 1–16.

[6] Jean-Paul Yehouessi et al. "Design and realization of flexible very large mode area pixelated Bragg fibers". In: *Optics Letters* 40.3 (2015), pp. 363–366.

[7] Assaad Baz et al. "Pixelated high-index ring Bragg fibers". In: *Optics Express* 20.17 (2012), pp. 18795–18802.

[8] Pochi Yeh, Amnon Yariv, and Emanuel Marom. "Theory of Bragg fiber". In: *JOSA* 68.9 (1978), pp. 1196–1201.

[9] J-P Yehouessi et al. "Ultra large mode area pixelated Bragg fiber". In: *Fiber Lasers XIII: Technology, Systems, and Applications*. Vol. 9728. SPIE. 2016, pp. 98–103.

[10] Jens Limpert et al. "Yb-doped large-pitch fibres: effective single-mode operation based on higher-order mode delocalisation". In: *Light: Science & Applications* 1.4 (2012), e8–e8.

[11] Siddharth Ramachandran et al. "Ultra-large effective-area, higher-order mode fibers: a new strategy for high-power lasers". In: *Laser & Photonics Reviews* 2.6 (2008), pp. 429–448.

[12] Xiongwei Hu et al. "All fiber MZ interferometer for high temperature sensing based on a hetero-structured cladding solid-core photonic bandgap fiber". In: *Optics Express* 24.19 (2016), pp. 21693–21699.

[13] JP Yehouessi et al. "Low-loss large mode area pixelated and heterostructured Bragg Fiber". In: *The European Conference on Lasers and Electro-Optics*. Optica Publishing Group. 2015, CJ_3_6.

[14] Cesar Jauregui, Jens Limpert, and Andreas Tünnermann. "High-power fibre lasers". In: *Nature photonics* 7.11 (2013), pp. 861–867.

[15] Xiuquan Ma et al. "Single-mode chirally-coupled-core fibers with larger than 50μm diameter cores". In: *Optics express* 22.8 (2014), pp. 9206–9219.

[16] Ritesh Kumar Chourasia. *Bragg Fibers: From Optical Properties to Applications*. Springer Nature.

[17] Zhen Xing et al. "Large mode area double-layer all-solid anti-resonant fiber for high-power fiber lasers". In: *Results in Physics* 29 (2021), p. 104700.

[18] Xia Yu et al. "Optical Fibers for High-Power Lasers". In: *Handbook of Optical Fibers; Peng, GD, Ed.; Springer: Singapore* (2018).

[19] A Malinowski et al. "High-peak-power, high-energy, high-average-power pulsed fiber laser system with versatile pulse duration and shape". In: *Optics Letters* 38.22 (2013), pp. 4686–4689.

[20] Gediminas Račiukaitis. "Ultra-short pulse lasers for microfabrication: a review". In: *IEEE Journal of Selected Topics in Quantum Electronics* 27.6 (2021), pp. 1–12.